Published in final edited form as:
Sci Immunol. 2018 November 30; 3(29): . doi:10.1126/sciimmunol.aau6598.

Intrinsic properties of human germinal-center B cells set antigen-affinity thresholds

Kihyuck Kwak[1], **Nicolas Quizon**[1], **Haewon Sohn**[1], **Avva Saniee**[1], **Javier Manzella-Lapeira**[1], **Prasida Holla**[1], **Joseph Brzostowski**[1], **Jinghua Lu**[1], **HengYi Xie**[2], **Chenguang Xu**[2], **Katelyn M. Spillane**[3,4,5], **Pavel Tolar**[4,5], and **Susan K. Pierce**[1,*]

[1]Laboratory of Immunogenetics, National Institute of Allergy and Infectious Diseases, National Institutes of Health, Rockville, Maryland 20852, USA

[2]MOE Key Laboratory of Protein Sciences, Collaborative Innovation Center for Diagnosis and Treatment of Infectious Diseases, School of Life Sciences, Institute for Immunology, Tsinghua University, Beijing, China

[3]Department of Physics, King's College London, London WC2R 2LS, UK

[4]Immune Receptor Activation Laboratory, The Francis Crick Institute, London NW1 1AT, England, UK

[5]Division of Immunology and Inflammation, Imperial College London, London SW7 2AZ, England, UK

Abstract

Protective antibody responses to vaccination or infection depend on affinity maturation, a process by which high-affinity germinal center (GC) B cells are selected based on their ability to bind, gather and present antigen to T follicular helper (Tfh) cells. Here we show that human GC B cells have intrinsically higher affinity thresholds for both B cell antigen receptor (BCR) signaling and antigen gathering as compared to naïve B cells and that these functions are mediated by distinct cellular structures and pathways that ultimately lead to antigen-affinity- and Tfh cell-dependent differentiation to plasma cells. GC B cells bound antigen through highly dynamic, actin- and ezrin-rich pod-like structures that concentrated BCRs. The behavior of these structure was dictated by the intrinsic antigen-affinity thresholds of GC B cells. Low affinity antigens triggered continuous engagement and dis-engagement of membrane associated antigens whereas high affinity antigens induced stable synapse formation. The pod-like structures also mediated affinity-dependent antigen internalization by unconventional pathways distinct from those of naïve B cells. Thus, intrinsic properties of human GC B cells set thresholds for affinity selection.

[*]To whom correspondence should be addressed: Susan K. Pierce, 5625 Fishers Lane, Room 4S04, Rockville, MD 20852 USA, spierce@nih.gov, Phone: (301) 496-9589; Fax: (301) 594-9990.

Author Contributions

K.K. and S.K.P. conceived and designed the study. K.K., N.Q., H.S., A.S., P.H., and J.L., performed experiments. K.K., N.Q., H.S., A.S., J.M., J.B., J.L., H.X., and C.X. analyzed data and performed statistical analysis. K.M.S., P.T. prepared DNA force sensor. K.K. wrote the original manuscript. N.Q., H.S., and S.K.P. edited the original manuscript. S.K.P. led the study.

Declaration of Interests

The authors declare no competing interests.

Europe PMC Funders Author Manuscripts

Europe PMC Funders Author Manuscripts

Introduction

A hallmark of immunological memory is the affinity maturation of antibody responses (1, 2). Underlying affinity maturation is the stochastic process of somatic hypermutation (SHM) and the subsequent competitive selection of B cells that have acquired affinity-enhancing mutations for the immunizing antigen or invading pathogen (2–5). The processes of SHM and affinity-based selection occur in spatially-distinct, specialized microenvironments within B cell follicles of secondary lymphoid organs termed germinal center (GC) dark zones (DZ) and light zones (LZ), respectively (5–7). Naïve B cells first encounter antigens in B cell follicles on the surfaces of subcapsular sinus macrophages, dendritic cells (DC), or follicular dendritic cells (FDC) (8, 9) triggering BCR signaling and antigen extraction, internalization, processing and presentation of the antigen on MHC class II molecules (4, 10). B cells then migrate to the border of the follicles with the T cell zone where they present antigen to T cells that have been recently primed by antigen presented on DCs to differentiate into T follicular helper (Tfh) cells (11, 12). The resulting B cell-Tfh cell interaction has the potential to drive B cells to several fates including differentiation to GC cells (13–16). GC B cells first enter GC DZs where they proliferate and undergo SHM prior to entering the GC LZs where antigen-affinity based selection occurs (17–19). Current evidence indicates that GC LZ selection is a competitive process dependent in large part on the amount of antigen B cells are able to gather, process and present to Tfh cells (20). LZ GC B cells have several potential fates that depend on their interactions with Tfh cells including, apoptosis, positive selections for re-entry into the DZ for further proliferative expansion and SHM or differentiation into MBCs or long-lived PCs (6).

Thus, there appear to be at least two key checkpoints in the process of affinity maturation, one for naïve B cells and one for LZ GC B cells. At these checkpoints, the affinity of B cells for antigen is tested by the ability of the BCR to differentially signal in response to and internalize, process and present antigen to T cells. However, despite the central role of these checkpoints in affinity selection and maturation we have a limited understanding of the potential of human naïve or GC B cells at these checkpoints to discriminate antigen affinity or of the cellular and molecular mechanisms that facilitate affinity discrimination by naïve and GC B cells. Here we describe intrinsic properties of human GC B cells that set thresholds for affinity selection providing a mechanistic framework for antigen affinity discrimination by GC B cells.

Results

GC B Cells Engage Antigen through BCRs Concentrated in Unconventional F-Actin and Ezrin-Rich Pod-like Structures

To understand how human naïve and GC B cells engage membrane-associated antigens, we obtained differential interference contrast (DIC) and interference reflection microscopy (IRM) images of live B cells isolated from human tonsils and placed on antigen-containing membranes (Fig. 1A and Movie S1). B cell subpopulations were purified from single cell suspensions of human tonsils B cells obtained by negative selection and sorted based on expression of CD10, IgD and CXCR4 into the four B cell subpopulations (fig. S1); naïve B cells (IgD^+ $CD10^-$); MBCs (IgD^- $CD10^-$); LZ GC B cells (IgD^- $CD10^+$ $CXCR4^{Lo}$) and DZ

GC B cells (IgD^{-} $CD10^{+}$ $CXCR4^{Hi}$). To further characterize these purified subpopulations we quantified the cell surface expression of the BCR by flow cytometry using fluorescently conjugated antibodies specific for either the λ or κ light chains. Naïve B cells expressed the highest level of BCR followed by MBCs, LZ GC and DZ GC B cells (fig. S2A). The expression of IgM, IgG, IgA isotypes was also lower on GC B cells (fig. S2B). As a surrogate membrane-associated antigen we used streptavidin-conjugated $F(ab')_2$ light chain-specific antibodies (anti- λ/κ) attached to biotinylated lipids incorporated into fluid planar lipid bilayers (PLBs). When placed on antigen-containing PLB naïve B cells appeared to form large flat, stable contact areas with the antigen-containing PLB and maintain active ruffling around the cell's periphery consistent with conventional immune synapses (Fig. 1A and Movie S1). The stable interaction on the naïve B cell with the bilayer over time was quantified and shown as a kymograph (Fig. 1B). The behavior of the LZ GC B cells on the antigen bilayer was remarkably different. Rather than forming flat stable contact areas, the cells touched the bilayer through highly dynamic, large pod-like structures (Fig. 1A and Movie S1). This behavior is displayed as a kymograph showing the dynamic movement of the cell over time (Fig. 1B). In the absence of antigen, the LZ GC B cell surfaces were smooth and the cells made contact with the bilayer through a small, stable area as evident in the IRM images (Fig. 1A and Movie S1). We extended the IRM analyses to include a comparison of DZ GCs in addition to naïve and LZ GC B cells. Naïve B cells rapidly responded to the antigen-containing PLB forming flat contact areas in uniform close proximity to the membrane that were stable over 20 min (Fig. 1C and Movie S2). In contrast, both DZ and LZ GC B cells made small, transient, highly dynamic contacts with the antigen-containing PLB for several minutes before the contacts stabilized but never reached the same high-intensity, uniform contact areas observed for naïve B cells. Quantification of the IRM images by several methods, including the intensity of the image from the center of the contact area to the edge (fig. S2C), the percent change in intensity from frame to frame (fig. S2D) and the number of contact sites over time (fig. S2E), supported the conclusion that naïve B cells rapidly formed uniform contact with the antigen-containing PLB in contrast to GC B cells that contacted the PLB in highly dynamic small points over several minutes.

To determine a role of actin in antigen-contact, we used super resolution stimulated emission depletion (STED) microscopy to obtain nanoscale images of the organization of F-actin in naïve and LZ GC B cells placed on antigen-containing PLBs for 25 min, fixed, permeabilized and stained with Alexa Fluor 488-conjugated phalloidin (Fig. 1D). The high-resolution images showed that naïve B cells formed conventional mesh-like F-actin structures in the contact area with weak actin signal intensity. In contrast, LZ GC B cells showed a high intensity punctate pattern of F-actin-rich structures primarily in the cell's periphery. Colocalization of the BCR and F-actin in the area of contact indicated that in contrast to naïve B cells, for which BCR clusters were not directly associated with polymerized F-actin (Fig. 1E) BCRs were associated with actin-rich structures in LZ GC B cells (Fig. 1E).

We also determined the amount of ezrin concentrated in the contact area of the B cells with the antigen-containing PLB and the degree of colocalization of ezrin with F-actin by confocal microscopy. Ezrin is a cytoplasmic peripheral membrane protein that is enriched in

actin-rich cell surface projections (21–23) and regulates morphological and cytoskeletal changes in B cells (24). By flow cytometry ezrin expression in GC B cells was approximately 10 fold higher as compared to naïve B cells (fig. S2F). In naïve B cells ezrin was primarily in the cell periphery where ezrin and F-actin were only partially colocalized (Fig. 1F). In contrast in LZ GC B cells ezrin was concentrated in a punctate pattern and was more highly colocalized with F-actin (Fig. 1F) suggesting that the GC B cell pod-like structures were both actin- and ezrin-rich.

Confocal Z-stack 3D images of cross sections of naïve and LZ GC B cells placed on antigen-containing PLBs revealed remarkable details of cellular architecture in the contact area that was consistent with the DIC, IRM, STED and confocal images (Fig. 1G). Naïve B cells formed contact with the antigen-containing PLB in a single plane in close opposition to the PLB resulting in a relatively uniform distribution of BCRs under a plane of F-actin. In contrast, LZ GC B cells contacted the antigen-containing PLB through actin-rich pod-like structures the tips of which concentrated BCRs. The dimensions of these structures were approximately 0.2-0.5um in diameter by 1.5um in length, much larger than microvilli through which T cells have been recently demonstrated to search for antigen (25). These structures were also evident by scanning electron microscopy (SEM) (Fig. 1H). By SEM, in the resting state, LZ GC B cells and naïve B cells showed distinct morphologies with LZ GC B cells having a corrugated membrane topology with long, thin protrusions, whereas naïve B cells had smoother membranes with short, thick bulges. More pronounced differences were observed between naïve B cells and LZ GC B cells that were activated on antigen-coated PLBs. Naïve B cells showed a flat area of contact with the bilayer visible in SEM in both top and side views in contrast to LZ GC cells in which pod-like contacts were visible in the side view.

The observation that BCRs were concentrated in the area of contact of the pod-like structures with the antigen-containing PLB predicted that antigen gathered from the PLB would also be concentrated in the contact areas of the pod-like structures. LZ GC B cells were placed on PLB containing fluorescently-labeled anti-λ/κ for 20 min and imaged. The DIC and antigen merged image clearly showed antigen concentrated at the ends of the pod-like structures (Fig. 1I).

Human GC B Cells Signal in Response to and Exert Pulling Forces on Membrane Bound Antigens through Pod-like Structures

BCRs were labeled with Alexa Fluor 488- or Alexa Fluor 647-Fab anti-IgM for naïve B cells or Alexa Fluor 488- or Alexa Fluor 647-Fab anti-IgG for GC B cells and B cells were placed on antigen-containing PLBs for 7 or 25 min. Cells were fixed, permeabilized and stained with fluorescently conjugated antibodies specific for the phosphorylated forms of kinases and phosphatases activated by the initiation of BCR signaling including PI3K and SHP-1 (Fig. 2A) and Syk, PLCγ2, Btk, Vav and Cbl (fig. S3A and S3B). Naïve B cells spread on the antigen-containing PLB over 25 min and pPI3K and pSHP-1 accumulated with BCRs in the contact area, forming a central cSMAC structure (Fig. 2A). In contrast, GC B cells did not form centralized BCR-pPI3K and -pSHP-1 clusters but rather pPI3K and pSHP-1 were concentrated with BCRs in a punctate pattern primarily in the cell periphery consistent with

BCRs signaling through podlike structures. Quantification of images showed that pPI3K and pSHP-1 were recruited earlier to naïve BCRs as compared to GC B cells but were more highly colocalized with the BCRs in GC B cells as compared to naïve B cells both in resting cells and at early and late phases of the response (Fig. 2B). Similarly, the colocalization of pSyk, pPLCγ2, pVav, pBtk, pCbl and CD19 with the BCR was consistently higher in GC cells as compared to naïve B cells (fig. S3B, S3C and Movie S3) but similar between IgM and IgG GC B cells (fig. S3D). Time-lapse live cell TIRFM imaging of the growth of individual BCR microclusters showed that microclusters grew rapidly on naïve B cells whereas growth of GC B cell BCR microclusters was slower (fig. S3E).

We also compared the ability of LZ and DZ GC B cells and naïve B cells to exert a pulling force on membrane antigen. To do so we used F(ab')2 anti-κ/λ as a surrogate antigen conjugated to a 9 pN DNA-based force sensor attached to PLBs (fig. S4A). The force sensor contained a central DNA hairpin that unwinds when pulling forces are exerted by the BCR on the antigen, displacing an Atto 647N dye from a dark quencher at the base of the hairpin resulting in increased Atto 647N fluorescence over the fluorescence of a force insensitive dye Atto 550 attached to the double stranded DNA at the top of the sensor. Opening is expressed as the ratio of the signal intensity of Atto 647N to that of Atto 550. Control sensors lack the hairpin and cannot be opened by force.

Time-lapse TIRFM imaging of the sensor's Atto 550 fluorescence showed that naïve B cells rapidly spread over the PLB capturing the sensor and accumulating it in the center of the contact area within 3 to 4 min, forming a flat immune synapse where the sensor persisted for several min (Fig. 2C and Movie S4). Quantification of the sensor opening showed that naïve B cells were unable to exert a force sufficient to open the sensor (Fig. 2D and Movie S4). LZ GC B cells showed a punctate pattern of clustered intensity consistent with the sensor binding to BCR concentrated in the pod-like structures. We observed robust Atto 647N intensity that coincided with areas of Atto 550 intensity (Fig. 2C), indicating that LZ GC B cells were able to exert a pulling force on the antigen of at least 9 pN through the pod-like structures. Analysis of DZ GC B cells showed a similar result.

To confirm that the LZ GC B cell's pulling force was exerted by the BCRs in the actin-rich pod-like structures, we simultaneously acquired images of the antigen-force sensors opening and IRM images and merged the two. LZ GC B cells exerted force on the sensors beginning approximately 5 min after the cells were placed on the sensor-containing PLBs and the opening of the sensors was restricted to the areas of contact of the LZ GC B cell's pod-like structures with the membrane (Fig. 2E and Movie S5).

Behavior of GC B Cells in Response to Antigen is Dictated by Intrinsic Affinity Thresholds

We determined if naïve and GC B cells were able to discern affinity for membrane-associated antigens. As surrogate antigen we used κ-specific monoclonal antibodies (anti-κ mAbs) that were generated in mice to either rat κ chains and showed a low-affinity for human κ chains ($KD = 3.9 \times 10^{-7}$) as determined by Biacore surface plasmon resonance analysis or were generated in mice to human κ chains and showed a high-affinity for human κ chains ($KD = 2.4 \times 10^{-9}$). Streptavidin conjugated anti-κ mAbs were bound to PLBs that contained biotinylated lipids. Lambda light chain-expressing B cells were removed from

purified naive B cell and LZ GC B cell sub-populations by negative sorting. The κ light chain-expressing LZ GC and naïve B cells were placed on PLBs that contained low- or high-affinity anti-κ mAbs for 7 or 25 min. Cells were permeabilized and stained with antibodies specific for the phosphorylated forms of the BCR's Igα chain, CD79a (pCD79A), and several components of the B cell signaling cascade including Syk (pSyk), BLNK (pBLNK) and PLCγ2 (pPLCγ2). Cells were imaged by TIRFM and the MFI in the contact areas between the B cell and the antigen-containing PLBs was quantified.

The TIRFM images showed that naïve B cells formed immune synapses similarly on both the high and low-affinity antigen-containing PLBs (Fig. 3A) and accumulated similar amounts of BCR in the area of contact between the B cell and the PLB in response to low and high-affinity antigens at 7 min (Fig. 3B). At 25 min, the accumulation of the BCR was less for low versus high-affinity antigens, nonetheless the accumulation was significantly greater than that of resting naïve B cells (Fig. 3B). In contrast, LZ GC B cells did not form stable contacts with the low-affinity antigen-containing bilayers (Fig. 3A) nor did they accumulate BCRs in the contact area between the B cell and the PLBs to an amount that was significantly greater than that accumulated by resting LZ GC B cells placed on bilayers that did not contain antigen (Fig. 3B). When placed on the high-affinity antigen-containing PLBs, LZ GC B cells accumulated BCRs in a punctate pattern (Fig. 3A). The amount of LZ GC BCRs that accumulated in the interface between the B cell and the high-affinity antigen-containing PLB was significantly greater than that of resting LZ GC B cells not exposed to antigen although less than that of naïve B cells (Fig. 3B).

Quantification of the phospho-signaling components in the contact area of the B cells with the bilayers showed a similar pattern. Naïve B cells induced phosphorylation of CD79a, Syk, BLNK and PLCγ when placed on either low-affinity or high-affinity antigen-containing PLBs (Fig. 3C-3F). In contrast, LZ GC B cells were unable to initiate phosphorylation of signaling components in response to low-affinity antigen-containing PLB (Fig. 3C-3F) but responded to high-affinity antigen-containing PLB. Also shown are both the DIC and IRM images (Fig. 3G and Movie S6) as well as quantitative analyses of both the IRM and DIC images displayed as kymographs (Fig. 3H). High-affinity antigens immobilized naïve B cells in stable large contact areas with the PLB (Fig. 3G and Movie S6) as quantified in the kymograph (Fig. 3H). In contrast, naïve B cells on low-affinity antigen-PLB formed smaller contact areas and continued to extend membrane ruffles around the periphery presumably continuing to search for antigen (Fig. 3G and Movie S6) as indicated by red arrow heads in the kymograph (Fig. 3H). LZ GC B cells placed on high-affinity antigen-containing PLB vigorously explored the PLB through their peripheral pods (Fig. 3H and Movie S6). However, with time their pod formed stable contacts with the PLB as indicated by the red arrow heads in the kymograph (Fig. 3H). Low-affinity LZ GC B cells failed to form stable contacts with the membranes but rather continued to make highly dynamic contacts with the PLBs (Fig. 3G, 3H and Movie S6) even occasionally moving over the PLB (Movie S7). Thus, the behavior of the B cells on the antigen-containing bilayers appears to be dictated by the B cells' affinity for antigen.

To quantify the movement of pod-like structures in the DIC images, individual pod-like structures on PLBs were identified and their movement was measured using a particle

tracking algorithm (fig. S4B). During the early stage of contact, LZ GC B cells engaged with high-affinity antigen moved their pods more vigorously in a broader area (median diffusion $2.5x10^{-3}$ um^2/sec) relative to LZ GC B cells engaged with low-affinity antigen (median diffusion $1.7x10^{-3}$ um^2/sec) (Fig. 3I). Movement of pod-like structures markedly slowed during the late stage of contact for LZ GC B cells engaged with high-affinity antigen (median diffusion $1.0x10^{-3}$ um^2/sec) relative to earlier time points and to LZ GC B cells engaged with low affinity antigen (median diffusion $1.3x10^{-3}$ um^2/sec) (Fig. 3I), indicating that as more BCRs engage with high-affinity antigen, pod movement stabilizes.

Extraction and Trafficking of Membrane Associated Antigen Distinguishes GC B cells

We tested the ability of GC B cells and naïve B cells to extract antigen from pliant plasma membrane sheets (PMS) presenting either high- or low-affinity anti-κ mAbs. Total purified human tonsil B cells were incubated on PMS coated with fluorescently labeled high- or low-affinity anti-κ for 2 h and the B cells were harvested and analyzed by flow cytometry to identify B cells that had acquired fluorescent antigen and within this population to identify naïve B cells and GC B cells (Fig. 4A). Naïve B cells acquired similar amounts of antigen from high-affinity and low-affinity PMS. In contrast, significantly fewer GC B cells acquired antigen from the low-affinity PMS as compared to the high-affinity PMS (Fig. 4A).

We characterized the patterns of trafficking and internalization of membrane associated antigen captured by BCRs of LZ GC B cells and naïve B cells placed on PLB that contained Atto 633-labeled antigen, fixed, permeabilized, and stained with Alexa Fluor 488-conjugated phalloidin. On naïve B cells antigen-bound BCRs accumulated in the plane of the contact area with the PMS in the center of the synapse where they were internalized (Fig. 4B and Movie S8). No cell surface associated antigen was detected outside of the contact area as shown in the 3D surface reconstruction (Fig. 4B). In contrast, LZ GC B cells engaged antigens via pod-like structures and trafficked antigen away from the contact area along the sides of the cells to distal sites for internalization (Fig. 4B and Movie S8). To determine the polarity of the cells we located the microtubule organizing centers (MTOCs) using γ tubulin-specific antibodies in naïve and LZ GC B cells after activation on antigen-containing PMS. In the majority of activated naïve B cells MTOCs were polarized and located proximal to PMS (Fig. 4C). In contrast, MTOCs in activated LZ GC B cells were not polarized toward the PMS and appeared to be dispersed large distances from the PMS (Fig. 4C).

BCR-mediated antigen internalization in B cells is primarily by clathrin-mediated endocytosis (CME) (26). Sorting nextin (SNX) 9 and SNX18 are key components of the endocytosis machinery and modulators of CME (27–29). By flow cytometry, the expression of both SNX9 and SNX18 was four to six fold higher in naïve B cells as compared to LZ GC B cells (fig. S5A and S5B). By confocal microscopy in naïve B cells both SNX9 and SNX18 were concentrated with antigen in the immune synapse (Fig. 4D), polarized toward the antigen-containing PMS as shown and quantified in longitudinal sections (Fig. 4D and fig. S5C-S5E). In striking contrast, in LZ GC B cells SNX9 and SNX18 showed no pattern of accumulation but rather were dispersed throughout the cell (Fig. 4D). In addition, 3D reconstructions of images of α-tubulin, SNX9 or 18 and antigen clearly showed the polarization of α-tubulin and SNX9 and 18 toward the contact area of naïve B cells with the

antigen-containing PLB and antigen internalization from the contact site (Fig. 4E and Movie S9). In contrast, α-tubulin and SNX9 and 18 were not polarized in LZ GC B cells and the antigen was trafficked along the outside of the cell to distal sites (Fig. 4E and Movie S9).

It has been shown, primarily in naïve mouse B cells, that extracted antigens are internalized and trafficked to specialized LAMP-1^+ MHC class II-containing late endosomes (MIIC) for antigen processing (30). In activated naïve B cells LAMP-1^+ vesicles were polarized toward the immune synapse and antigens gathered by BCRs were highly colocalized with LAMP-1^+ vesicles (Fig. 4F and Movie S10). LAMP-1^+ vesicles in LZ GC B cells were less polarized and less antigen was colocalized with LAMP-1^+ vesicles.

We next followed the trafficking of antigen internalized by naïve B cells and LZ GC B cells with time. Unsorted purified tonsil B cells were incubated on PMS containing DyLight 650-conjugated $F(ab')_2$ anti-λ/κ and the pH-sensitive dye, pHrodo, the FI of which increases with increasing pH. Cells were removed from the PMS and analyzed by flow cytometry to identify naïve B cells and LZ GC B cells and to quantify the DyLight 650 and pHrodo FI. In controls in which the PMS contained DyLight 650-conjugated BSA and pHrodo, no DyLight 650 or pHrodo FI was detected in naïve and LZ GC B cells (Fig. 4G). Between 30 and 120 min on the PMS the amount of antigen associated with naïve and LZ GC B cells increased as did the pHrodo FI, however, the temporal patterns of antigen up-take and pHrodo FI differed between naïve and LZ GC B cells (Fig. 4G). Overlapping the data in Fig. 4G it is apparent that naive B cells extracted more antigen with time as compared to LZ GC B cells (fig. S5F) and trafficked a larger portion of the acquired antigen to acidic compartments as indicated by increased pHrodo FI. Comparing naïve B cells to LZ GC B cells that acquired equivalent amounts of antigen at 120 min, it was clear that naïve B cells trafficked a larger portion of the antigen to acidic compartments: over 80% of naïve B cells were pHrodo positive as compared to 20% of LZ GC B cells and the pHrodo FI was higher for naïve B cells as compared to LZ GC B cells (Fig. 4H).

Human LZ GC B Cells Express IRF-4 in Response to High-Affinity Antigen in Combination with Tfh Cell Help

We characterized the response of naïve and LZ GC B cells to high versus low-affinity membrane bound antigens in the presence or absence of CD40-specific mAb, IL-4 and IL-21 to mimic Tfh cell help. We quantified the expression of IRF-4, a gene required for PC differentiation and found that LZ GC B cells increased transcription of IRF-4 modestly in response to high but not low-affinity antigens (Fig. 5A). However, the largest increase in IRF-4 expression was in response to a combination of high-affinity antigen and Tfh cell help. In contrast to LZ GC B cells, naïve B cells expressed IRF4 equivalently in response to both high and low-affinity antigens (Fig. 5B). Tfh cell help independently induced IRF4 expression and augmented the IRF4 expression to both low and high-affinity antigens. Taken together these data provide evidence that the high-affinity threshold for activation of LZ GC B cells as compared to naïve B cells has the functional outcome of maximally triggering high-affinity LZ GC B cells to differentiate to PCs in the presence of Tfh cell help.

Europe PMC Funders Author Manuscripts

The Differential Expression of Surface Markers may Further Contribute to Affinity Discrimination by Human GC B Cells

We carried out an analysis of over 330 B cell surface markers on resting and antigen-activated naïve B cells, DZ and LZ GC B cells and MBCs. The data are expressed as a heat map comparing LZ and DZ GC B cells and MBCs to naïve B cells (Fig. 6A and fig. S6). LZ GC and DZ GC B cells showed nearly identical cell surface expression profiles with the exception of a few previously reported markers including CD83, CD86, and CXCR4. In contrast, the cell surface expression of markers on MBC more closely resembled that of naïve B cells. Notably, many environmental sensing co-receptors involved in the regulation of BCR signaling were down-regulated in GC B cells including FcεRII, FcγRII, CR1, SIGLEC-2, PECAM-1 and CR2, suggesting that the response of GC B cells to antigen may be minimally influenced by environmental signals.

Integrins were also differentially expressed by GC B cells as compared to naïve B cells and given their importance in B cell activation, we quantified the expression levels of a variety of human integrins and found a significant difference between naïve B cells and LZ GC B cells in their expression of integrin alpha 4, alpha M, beta 1 and beta 7 (Fig. 6A, fig. S7A, and S7B). We further characterized VLA-4 expression as it plays a key role in stabilizing the initial interaction of B cells with antigens associated on the surface of APCs that express its ligand, VCAM-1 (31). VLA-4/VCAM-1 interactions also facilitate B cell activation following BCR antigen binding (31). As compared to naïve B cells, the surface expression of the VLA-4 chains CD29 (β1) and CD49d (α4) was greatly reduced on LZ GC B cells (Fig. 6B and 6C) as was VLA-4 in the high-affinity state (Fig. 6B and 6C) (31).

To determine if the decreased expression of VLA-4 resulted in a reduced ability of GC B cells to adhere to VCAM-1 on surfaces, we incubated unsorted purified tonsillar B cells with an excess of VCAM-1-coated magnetic agarose beads at 37°C for 20 min and analyzed the composition of bead-bound and unbound B cells by flow cytometry. The vast majority of B cells that bound to the VCAM-1 beads were naïve B cells (Fig. 6D). GC B cells were nearly exclusively recovered in the unbound fraction indicating that the low expression of VLA-4 on GC B cells had the functional consequence of limiting the ability of GC B cells to engage VCAM-1 surfaces. Taken together these results suggest that GC B cells may be highly dependent on BCR-antigen interactions in the absence of strong integrin mediated cell-cell contact with antigen presenting cells.

Discussion

We determined that, as compared to human naïve B cells, human GC B cells have a higher intrinsic affinity threshold for antigen. We observed that independently of other extrinsic factors, such as competition among B cells for antigen, the intrinsic affinity of GC B cells for an antigen dictated each subsequent step in B cell activation from the magnitude of BCR signaling to the receptivity of BCR-stimulated GC B cells to Tfh cell signals that drive IRF4 expression and PC differentiation. We provided evidence that BCRs on LZ GC B cells are concentrated in distinct, highly dynamic, ezrin- and actin-rich pod-like structures through which the BCRs engage antigen, signal, exert pulling forces and extract antigen from membranes. In contrast, the BCRs on naïve B cells function in flat, stable membrane

contacts with antigen-containing surfaces displaying the well-described features of immune synapses and cSMACs. The role of these pod-like structures in establishing high affinity thresholds for GC B cells is at present a matter of speculation. These structures could serve to isolate small numbers of GC B cells reducing the B cells avidity for antigen forcing B cells to function through only monomeric affinity-dependent interactions as described earlier (32) or isolate BCRs from the trans-activity of BCR signaling molecules such as been described for Syk (33). On a larger size scale, the dynamic nature of the GC pod-like structures may underlie the rapid scanning behavior of LZ GC B cells over FDC observed *in vivo* in mice (9). We observed that LZ GC B cells engaging high-affinity antigen moved their pods more vigorously in broader areas as compared to LZ GC B cells engaging low-affinity antigen, suggesting that LZ GC B cells modulate their search for antigen in response to BCR affinity. Our results indicate that GC B cells isolated from tonsils have already established a high affinity threshold for antigen allowing only cells that meet or exceed this threshold to be selected. As the threshold appears to be an intrinsic feature of GC B cells, increases in antibody affinity with time could reflect a re-setting of the threshold for example in LZ GC B cells that re-enter the GC DZ.

We also observed striking differences in the internalization and the intracellular trafficking of antigen to acidic compartments for processing. For example, we observed that naïve B cells acquired more antigen with time as compared to GC B cells and immediately delivered a greater portion of their acquired antigen to acidic compartments for processing. In contrast, only a small portion of GC B cells that acquired a similar amount of antigen were able to traffic antigen into acidic compartments. The high threshold for processing of internalized antigen may provide a mechanism by which GC B cells temporally or spatially regulate the presentation of antigen to Tfh cells during GC LZ competition.

In terms of the outcome of LZ GC B cell encounter with antigen, we demonstrated that LZ GC B cells optimally increased IRF-4 transcription in response to high-affinity antigen and Tfh-like stimuli. In mice it has been shown that sustained high expression of IRF4 promote PC differentiation (34–37). Our observation is consistent with the findings of Krautler *et al.* (38) that provided evidence in mice for a two-signal mechanism in the differentiation of LZ GC B cells to PCs, the first provided by antigen and the second by Tfh cells. In contrast to LZ GC B cells, increases in IRF-4 expression in naïve B cells was relatively affinity-independent and more highly dependent on Tfh cell help suggesting that low-affinity B cells may capture sufficient antigen to activate Tfh cells to allow differentiation directly to short-lived PCs *in vivo*. The expression of CD40, IL4R, and IL21R in GC B cells was slightly higher than naïve B cells (fig. S6C) which could contribute to higher IRF4 mRNA expression in GC B cells as compared to naïve B cells in response to Tfh-like stimuli alone. However, the induction of IRF4 mRNA expression was antigen-affinity dependent only in GC B cells.

We also provided evidence for a variety of additional differences between GC B cells and naïve B cells that together could further contribute to establishing antigen affinity thresholds. For example, we showed that as compared to naïve B cells human LZ GC B cells express very little VLA-4 which is unique in human GC B cells as mouse GC B cells show comparable surface expression level of VLA-4 in comparison with naïve B cells (39).

VLA-4 is an integrin that binds to its ligand, VCAM-1, expressed by FDCs that present antigen to LZ GC B cells and serves to lower the affinity threshold for BCR signaling. It is of interest that in contrast to VLA-4 the expression of which was decreased on LZ GC B cells as compared to naïve B cells, the levels of expression of LFA-1 were similar for LZ GC B cells and naïve B cells. LFA-1 is an integrin that both stabilizes B cell interactions with APCs and plays a critical role in B cell-T cell interactions (40). This suggests that once LZ GC B cells succeed in triggering BCR signaling in a mostly VLA-4-independent fashion, the GC B cells will not be compromised in subsequent LFA-1-dependent processes, including interactions with Tfh cells.

In the studies described here we limited our analysis to a comparison of GC B cells and naïve B cells. It will be of interest in future studies to understand the mechanisms by which MBCs that have undergone affinity selection in GCs discriminate antigen affinity. Wang *et al.*41 recently reported that in mice GCBs expressing IgG BCRs generated greater traction forces on membrane-associated antigen during the initiation of activation than did naïve B cells consistent with increased expression of motor proteins in MBCs. Preliminary results from our studies are consistent with this observation showing that MBCs were able to exert pulling force on membrane-associated antigen that was sufficient to open 9 pN DNA force sensor whereas naïve B cells were not. How this function of MBCs might contribute to affinity discrimination remains to be determined. Our studies here were limited to κ-specific mAbs serving as surrogate antigens that differed approximately 60 fold. It will be of interest to develop additional reagents that allow a more precise assessment of the degree of affinity discrimination of these two human B cell subsets.

Our studies presented here provided evidence for intrinsic properties of LZ GC B cells that may contribute to enhanced affinity discrimination. Further elucidating the mechanisms of affinity discrimination may provide new strategies for the development of vaccines which require the generation of affinity-matured antibody responses.

Materials and Methods

Purification and sorting of human tonsil B lymphocytes

Tonsils were obtained from patients undergoing tonsillectomies. B cells were isolated from tonsil single tonsil cell suspensions by negative selection using the EasySep Human B cell enrichment kit (STEMCELL) and when indicated were sorted to obtain populations of naïve, MBC and LZ and DZ GC B cells staining with fluorescently labeled anti-IgD, anti-CD10, anti-CD184 anti-λ using a FACSAria II cell sorter (BD Biosciences).

Microscopy

PLBs containing either goat $F(ab')_2$ anti-human Igκ (SouthernBiotech) and anti-human Igλ (SouthernBiotech) or for affinity measurements anti-human Igκ or anti- rat Igκ as surrogate antigens were prepared as described (42). For fixed cell imaging, cells were stained with antibodies as indicated, place on PBL for the times indicated, fixed permeabilized in saponin, and stained with the appropriate antibodies to detect intracellular proteins. Images were acquired by Olympus IX-81 TIRF microscope system and analyzed by MatLab

(MathWorks) software. Pearson's correlation coefficients were calculated using MatLab software. Time-lapse live cell TIRF images were acquired at 6 sec intervals for 20 min as described for cells stained with antibodies as indicated. Time-lapse live cell DIC TIRF image acquisition and analysis was performed as previously described (43). Time-lapse live cell IRM TIRF images were acquired at 3 sec intervals for 20 min and MatLab algorithms were developed to perform automated image analysis as detailed in Supplementary Methods. BCR cluster growth was measured in live cell TIRF images by MatLab as described (43). For super resolution images of F-actin structure in the immune synapse, cells were stained with phalloidin (Thermo Fisher) and images were acquired by STED microscopy (Leica). SEM images were acquired from fixed samples coated with 5nm of gold in an EMS 575-X sputter coater (Electron Microscopy Sciences, Hatfield PA) and imaged with a Hitachi S-3400 N1 scanning electron microscope (Hitachi High Technologies America, Inc., Pleasanton CA). Confocal images were obtained using a Zeiss-880 confocal microscope and stacked images were deconvolved with Huygens Software (Huygens Software). The MFI and the Pearson's correlation coefficients of fluorescent proteins were calculated from background-subtracted images by Zen software (Zeiss). Distance of fluorescent proteins from PMS and MFI per each z-stack were measured by ImageJ (NIH). 3D images and movies and colocalizations were generated by Imaris (Bitplane)

Flowcytometry

To quantify cell surface marker expression, purified tonsillar B cells from five different individuals were stained with near-IR Live/Dead marker (Thermo Fisher) and fluorescently-labeled specific antibodies on ice, washed and analyzed by flow cytometry using a BD LSR II instrument and the data were analyzed using FlowJo (FLOWJO, LLC) and Prism (GraphPad) software. For quantification of intracellular proteins cells were fixed and permeabilized using BD Cytofix/Cytoperm (BD Biosciences) and incubated with fluorescently labeled specific antibodies at room temperature for 2 h, washed and when indicated cells were incubated with fluorescently labeled secondary antibodies, washed and analyzed.

VCAM-1 binding assay

Purified tonsil B cells were incubated with nickel agarose magnetic beads (Sigma) coated with recombinant human VCAM-1 Fc chimera proteins (R&D Systems) or purified human IgG (MP biomedicals) for 37°C for 30 min. Unbound cells were collected using a magnetic separation stand and bound cells were eluted from the beads with HBSS containing 150mM imidazole (Sigma) elution buffer. Cells were analyzed by flow cytometry (BD LSR II) and flow cytometry data was analyzed with FlowJo (FLOWJO, LLC) and Prism (GraphPad) software.

Detection and tracking of pod-like structures

Time-lapse live cell DIC and IRM images were acquired at 3 sec intervals for 20 min after placing cells on antigen-containing PLBs. Analyses of time-lapse acquisitions were performed with MatLab and ImageJ. Variations in intensity in DIC image sequences were normalized using linear regression in MatLab. Images were sharpened using an unsharp masking algorithm in MatLab to enhance the contrast of the pod-like structures. Pixels were

proportionately scaled down and binned into 8-bit unsigned integers to reduce the effects of small variations in pixel intensities. Masks were created using a method similar to topographic prominence in ImageJ by iteratively applying the Maximum function to identify the local intensity maximum of pod-like structures as a single point. Points were then tracked over time and their diffusion coefficients calculated using Matlab code developed to track single particles as described previously (32).

Measurement and analysis of pulling forces

Antigen conjugated force and control sensors were produced and measurement of sensor opening was conducted as described previously (44) using sensors containing goat $F(ab')_2$ anti-human Igκ and anti-human Igλ as surrogate antigens. For the movies, images were background subtracted and flatfield corrected in ImageJ (NIH) and value 1000 was added to Atto550 images before ratio calculation to reduce background. For statistical analysis, images were acquired after 20 min of incubation of the cells in antigen-containing PLB, background subtracted and flatfield corrected in ImageJ. Using the threshold function, the ratio of Atto647N to Atto550 fluorescence in antigen clusters of each cell was calculated by ImageJ and statistical analysis of sensor opening from each B cell subset was calculated by Prism software (Graphpad).

Antigen extraction and trafficking

To measure antigen extraction, PMSs containing either fluorescently labeled anti-human Igκ (GeneTex) or anti-rat Igκ (Thermo Fisher) were prepared as described (44). Cells were harvested and stained with near-IR Live/Dead marker (Thermo Fisher), anti-IgD Fab (SouthernBiotech), anti-CD10 (BD Biosciences), and the signal was quantified by flow cytometry (BD LSR II). To measure antigen trafficking, cells were placed on PMSs containing DyLight 550 and pHrodo avidin (Thermo Fisher) conjugated goat $F(ab')_2$ anti-human Igκ (SouthernBiotech) and anti-human Igλ (SouthernBiotech) as described above. Cells were harvested, stained with near-IR Live/Dead marker (Thermo Fisher), anti-IgD Fab (SouthernBiotech), anti-CD10 (BD Biosciences), and the signal was quantified by flow cytometry (BD LSR II).

Activation of naïve and LZ GC B Cells and measurement of IRF-4 mRNA expression

B cells were placed on PLB containing anti-human Igκ or anti- rat Igκ antibodies and incubated at 37°C with 5% CO_2 and 75% humidity for 1 h. RPMI-10 culture media containing anti-CD40 antibody (2ug/mL, R&D systems), IL-4 (40ng/mL, R&D systems), and IL-21 (2ug/mL Biolegend), or RPMI-10 culture media alone was added to the cells, cells were incubated at 37°C for an additional 2 h and harvested. Cells were lysed, RNA was reverse transcribed, and cDNA was used to run TaqMan Gene Expression Assays using TaqMan Gene Expression Cells-to-C_T kit (Thermo Fisher) on CFX connect Real-Time PCR Detection System (Bio Rad, check model name again). TaqMan Gene Expression Assays detecting IRF-4 (Hs00180031_m1, Thermo Fisher) and ACTB (Hs1060665_g1, Thermo Fisher) were used to measure levels of mRNA and ACTB was used for normalization. Data were analyzed by Prism software (GraphPad).

Measurement and analysis of surface molecule expression

Purified tonsil B cells from three different individuals were incubated at 37°C for 2 h with 10ug/ml of goat $F(ab')_2$ anti-human Igκ (SouthernBiotech) and anti-human Igλ (SouthernBiotech). Cells were then washed, stained with Live/Dead marker (Thermo Fisher), anti-CD19 (Biolegend), anti-IgD (Miltenyi), anti-CD10 (BD Biosciences), and anti-CD184 (BD Biosciences) and barcoded as described (45). Cells were washed, combined and further stained for surface markers using a LEGENDScreen (Biolegend) human cell screening kit. Fluorescent signals were quantified by flow cytometry (BD LSR II). Flow cytometry data was analyzed with FlowJo v.10.1 and Microsoft Excel 2016.

Supplementary Material

Refer to Web version on PubMed Central for supplementary material.

Acknowledgements

This work was supported by the Intramural Research Program of the National Institute of Health, National Institute of Allergy and Infectious Diseases. P.T. and K.S. were supported by the H2020 European Research Council (Consolidator Grant 648228) and the Francis Crick Institute, which receives its core funding from Cancer Research UK, the UK Medical Research Council, and the Wellcome Trust. Authors would like to thank DC-CFAR Basic Science Core and Children's National Medical Center (CNMC) for providing tonsil specimens. Data and materials are available from the corresoponding author upon request.

References

1. Eisen HN, Siskind GW. Variations in Affinities of Antibodies during the Immune Response. Biochemistry. 1964; 3:996–1008. [PubMed: 14214095]
2. De Silva NS, Klein U. Dynamics of B cells in germinal centres. Nat Rev Immunol. 2015; 15:137–148. [PubMed: 25656706]
3. Shlomchik MJ, Weisel F. Germinal center selection and the development of memory B and plasma cells. Immunol Rev. 2012; 247:52–63. [PubMed: 22500831]
4. Batista FD, Harwood NE. The who, how and where of antigen presentation to B cells. Nat Rev Immunol. 2009; 9:15–27. [PubMed: 19079135]
5. Shinnakasu R, Kurosaki T. Regulation of memory B and plasma cell differentiation. Curr Opin Immunol. 2017; 45:126–131. [PubMed: 28359033]
6. Mesin L, Ersching J, Victora GD. Germinal Center B Cell Dynamics. Immunity. 2016; 45:471–482. [PubMed: 27653600]
7. Bannard O, Cyster JG. Germinal centers: programmed for affinity maturation and antibody diversification. Curr Opin Immunol. 2017; 45:21–30. [PubMed: 28088708]
8. Carrasco YR, Batista FD. B cells acquire particulate antigen in a macrophage-rich area at the boundary between the follicle and the subcapsular sinus of the lymph node. Immunity. 2007; 27:160–171. [PubMed: 17658276]
9. Suzuki K, Grigorova I, Phan TG, Kelly LM, Cyster JG. Visualizing B cell capture of cognate antigen from follicular dendritic cells. J Exp Med. 2009; 206:1485–1493. [PubMed: 19506051]
10. Tolar P. Cytoskeletal control of B cell responses to antigens. Nat Rev Immunol. 2017; 17:621–634. [PubMed: 28690317]
11. Okada T, et al. Antigen-engaged B cells undergo chemotaxis toward the T zone and form motile conjugates with helper T cells. PLoS Biol. 2005; 3:e150. [PubMed: 15857154]
12. Qi H, Cannons JL, Klauschen F, Schwartzberg PL, Germain RN. SAP-controlled T-B cell interactions underlie germinal centre formation. Nature. 2008; 455:764–769. [PubMed: 18843362]

13. Jacob J, Kelsoe G. In situ studies of the primary immune response to (4-hydroxy-3-nitropheny1)acetyl. II. A common clonal origin for periarteriolar lymphoid sheath-associated foci and germinal centers. J Exp Med. 1992; 176:679–687. [PubMed: 1512536]
14. Taylor JJ, Pape KA, Jenkins MK. A germinal center-independent pathway generates unswitched memory B cells early in the primary response. J Exp Med. 2012; 209:597–606. [PubMed: 22370719]
15. Dal Porto JM, Haberman AM, Kelsoe G, Shlomchik MJ. Very low affinity B cells form germinal centers, become memory B cells, and participate in secondary immune responses when higher affinity competition is reduced. J Exp Med. 2002; 195:1215–1221. [PubMed: 11994427]
16. Shih TA, Meffre E, Roederer M, Nussenzweig MC. Role of BCR affinity in T cell dependent antibody responses in vivo. Nat Immunol. 2002; 3:570–575. [PubMed: 12021782]
17. Schwickert TA, et al. In vivo imaging of germinal centres reveals a dynamic open structure. Nature. 2007; 446:83–87. [PubMed: 17268470]
18. Allen CD, Okada T, Tang HL, Cyster JG. Imaging of germinal center selection events during affinity maturation. Science. 2007; 315:528–531. [PubMed: 17185562]
19. Hauser AE, et al. Definition of germinal-center B cell migration in vivo reveals predominant intrazonal circulation patterns. Immunity. 2007; 26:655–667. [PubMed: 17509908]
20. Victora GD, et al. Germinal center dynamics revealed by multiphoton microscopy with a photoactivatable fluorescent reporter. Cell. 2010; 143:592–605. [PubMed: 21074050]
21. Birgbauer E, Solomon F. A marginal band-associated protein has properties of both microtubule- and microfilament-associated proteins. J Cell Biol. 1989; 109:1609–1620. [PubMed: 2677023]
22. Goslin K, Birgbauer E, Banker G, Solomon F. The role of cytoskeleton in organizing growth cones: a microfilament-associated growth cone component depends upon microtubules for its localization. J Cell Biol. 1989; 109:1621–1631. [PubMed: 2677024]
23. Pakkanen R, Hedman K, Turunen O, Wahlstrom T, Vaheri A. Microvillus-specific Mr 75,000 plasma membrane protein of human choriocarcinoma cells. J Histochem Cytochem. 1987; 35:809–816. [PubMed: 3298422]
24. Parameswaran N, Matsui K, Gupta N. Conformational switching in ezrin regulates morphological and cytoskeletal changes required for B cell chemotaxis. J Immunol. 2011; 186:4088–4097. [PubMed: 21339367]
25. Cai E, et al. Visualizing dynamic microvillar search and stabilization during ligand detection by T cells. Science. 2017; 356
26. Stoddart A, Jackson AP, Brodsky FM. Plasticity of B cell receptor internalization upon conditional depletion of clathrin. Mol Biol Cell. 2005; 16:2339–2348. [PubMed: 15716350]
27. Soulet F, Yarar D, Leonard M, Schmid SL. SNX9 regulates dynamin assembly and is required for efficient clathrin-mediated endocytosis. Mol Biol Cell. 2005; 16:2058–2067. [PubMed: 15703209]
28. Haberg K, Lundmark R, Carlsson SR. SNX18 is an SNX9 paralog that acts as a membrane tubulator in AP-1-positive endosomal trafficking. J Cell Sci. 2008; 121:1495–1505. [PubMed: 18411244]
29. Park J, et al. SNX18 shares a redundant role with SNX9 and modulates endocytic trafficking at the plasma membrane. J Cell Sci. 2010; 123:1742–1750. [PubMed: 20427313]
30. Watts C. Antigen processing in the endocytic compartment. Curr Opin Immunol. 2001; 13:26–31. [PubMed: 11154913]
31. Carrasco YR, Batista FD. B-cell activation by membrane-bound antigens is facilitated by the interaction of VLA-4 with VCAM-1. EMBO J. 2006; 25:889–899. [PubMed: 16456548]
32. Tolar P, Hanna J, Krueger PD, Pierce SK. The constant region of the membrane immunoglobulin mediates B cell-receptor clustering and signaling in response to membrane antigens. Immunity. 2009; 30:44–55. [PubMed: 19135393]
33. Rolli V, et al. Amplification of B cell antigen receptor signaling by a Syk/ITAM positive feedback loop. Mol Cell. 2002; 10:1057–1069. [PubMed: 12453414]
34. Klein U, et al. Transcription factor IRF4 controls plasma cell differentiation and class-switch recombination. Nat Immunol. 2006; 7:773–782. [PubMed: 16767092]

35. Sciammas R, et al. Graded expression of interferon regulatory factor-4 coordinates isotype switching with plasma cell differentiation. Immunity. 2006; 25:225–236. [PubMed: 16919487]
36. Li X, et al. Cbl Ubiquitin Ligases Control B Cell Exit from the Germinal-Center Reaction. Immunity. 2018; 48:530–541 e536. [PubMed: 29562201]
37. Nutt SL, Hodgkin PD, Tarlinton DM, Corcoran LM. The generation of antibody-secreting plasma cells. Nat Rev Immunol. 2015; 15:160–171. [PubMed: 25698678]
38. Krautler NJ, et al. Differentiation of germinal center B cells into plasma cells is initiated by high-affinity antigen and completed by Tfh cells. J Exp Med. 2017; 214:1259–1267. [PubMed: 28363897]
39. Wang X, Rodda LB, Bannard O, Cyster JG. Integrin-mediated interactions between B cells and follicular dendritic cells influence germinal center B cell fitness. J Immunol. 2014; 192:4601–4609. [PubMed: 24740506]
40. Carrasco YR, Fleire SJ, Cameron T, Dustin ML, Batista FD. LFA-1/ICAM-1 interaction lowers the threshold of B cell activation by facilitating B cell adhesion and synapse formation. Immunity. 2004; 20:589–599. [PubMed: 15142527]
41. Wang J, et al. Profiling the origin, dynamics, and function of traction force in B cell activation. Sci Signal. 2018; 11
42. Liu W, et al. The scaffolding protein synapse-associated protein 97 is required for enhanced signaling through isotype-switched IgG memory B cell receptors. Sci Signal. 2012; 5:ra54. [PubMed: 22855505]
43. Wang J, Sohn H, Sun G, Milner JD, Pierce SK. The autoinhibitory C-terminal SH2 domain of phospholipase C-gamma2 stabilizes B cell receptor signalosome assembly. Sci Signal. 2014; 7:ra89. [PubMed: 25227611]
44. Nowosad CR, Spillane KM, Tolar P. Germinal center B cells recognize antigen through a specialized immune synapse architecture. Nat Immunol. 2016; 17:870–877. [PubMed: 27183103]
45. Akkaya B, et al. A Simple, Versatile Antibody-Based Barcoding Method for Flow Cytometry. J Immunol. 2016; 197:2027–2038. [PubMed: 27439517]

Europe PMC Funders Author Manuscripts

Europe PMC Funders Author Manuscripts

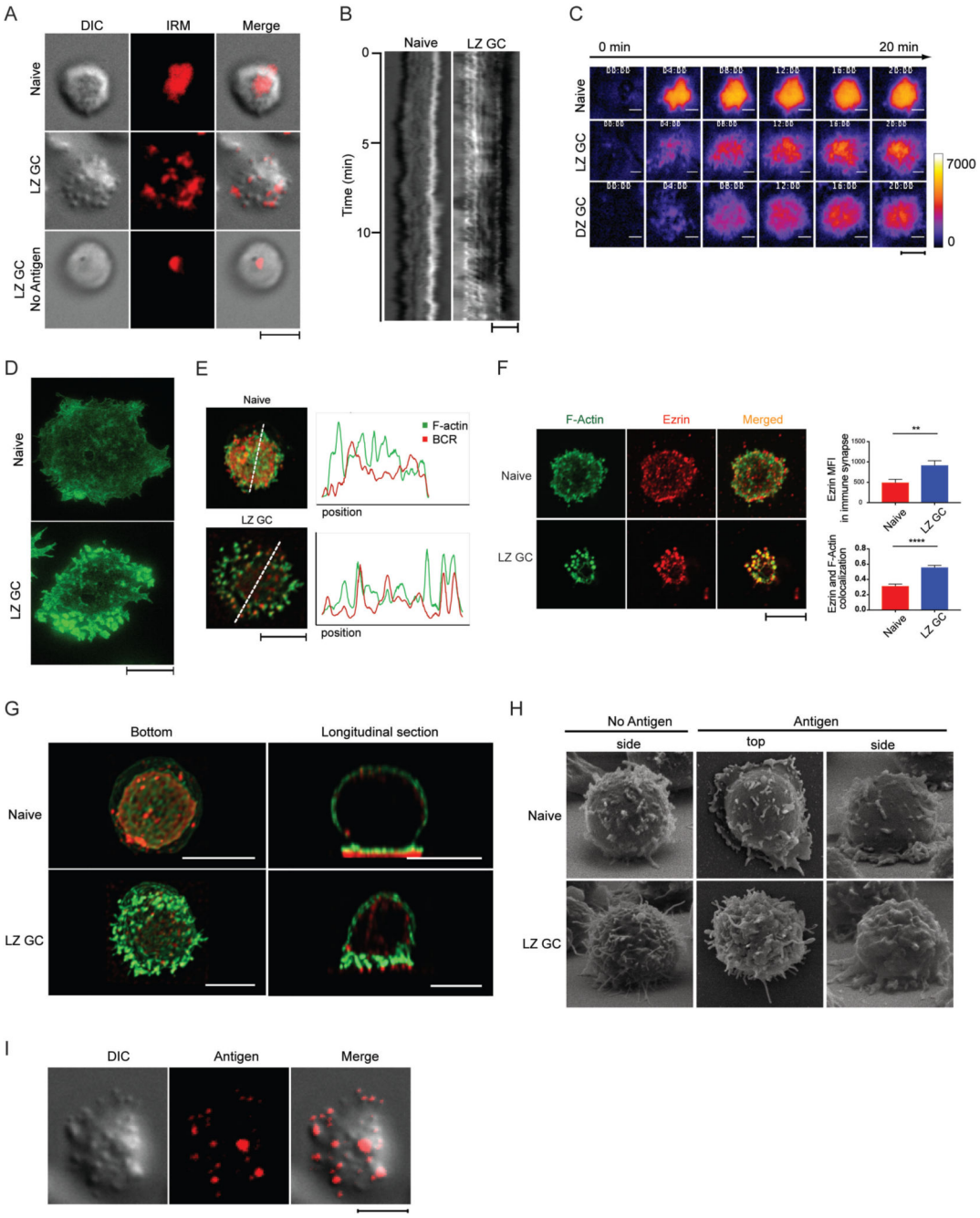

Figure 1.

GC B Cells Engage Antigen through BCRs Concentrated in F-Actin and Ezrin-Rich Pod-like Structures. **(A)** DIC, IRM, and merged images of immune synapse of live naïve B cells placed on antigen-containing PLB and live LZ GC B cells placed on antigen-containing PLB or PLB with no antigen. **(B)** Kymographs of DIC images of naïve and LZ GC B cell immune synapse on antigen-containing PLB. **(C)** Membrane movement in the immune synapses of live naïve, LZ GC, and DZ GC B cells with time on antigen-containing PLB imaged by IRM. **(D)** STED super-resolution images of F-actin formed in immune synapses of naïve B

cells and GC B cells placed on PLB that contained antigen. **(E)** Colocalization of F-actin and BCR in immune synapses of naïve and LZ GC B cells imaged by confocal microscopy on PLB that contained antigen. **(F)** (Left panel) Confocal microscopy images of immune synapses of naïve B cells and LZ GC B cells on antigen-coated PLB stained with Alexa Fluor 488 phalloidin for F-actin (green) and antibodies specific for ezrin (red). (Top right panel) Quantification of the MFI of ezrin and (Bottom right panel) colocalization of ezrin with F-actin (bottom) in the immune synapse of confocal images. **(G)** Bottom and orthogonal views of F-actin (green) and BCR (red) in naïve and LZ GC B cells imaged by confocal microscopy on antigen-containing PLB. **(H)** Side and top views of naïve and LZ GC B cells imaged by SEM on PLB without or with antigen. **(I)** Colocalization of pod-like structures and antigens in immune synapse of LZ GC B cells imaged by TIRFM on antigen-containing PLB. Scale bars are 5μm. *ns*>0.05, ***P*≤0.05, ****P*≤0.01, *****P*≤0.001, and ******P*≤0.0001 (unpaired *t*-test). Data are representative of two experiments (F: mean and s.e.m.).

Europe PMC Funders Author Manuscripts

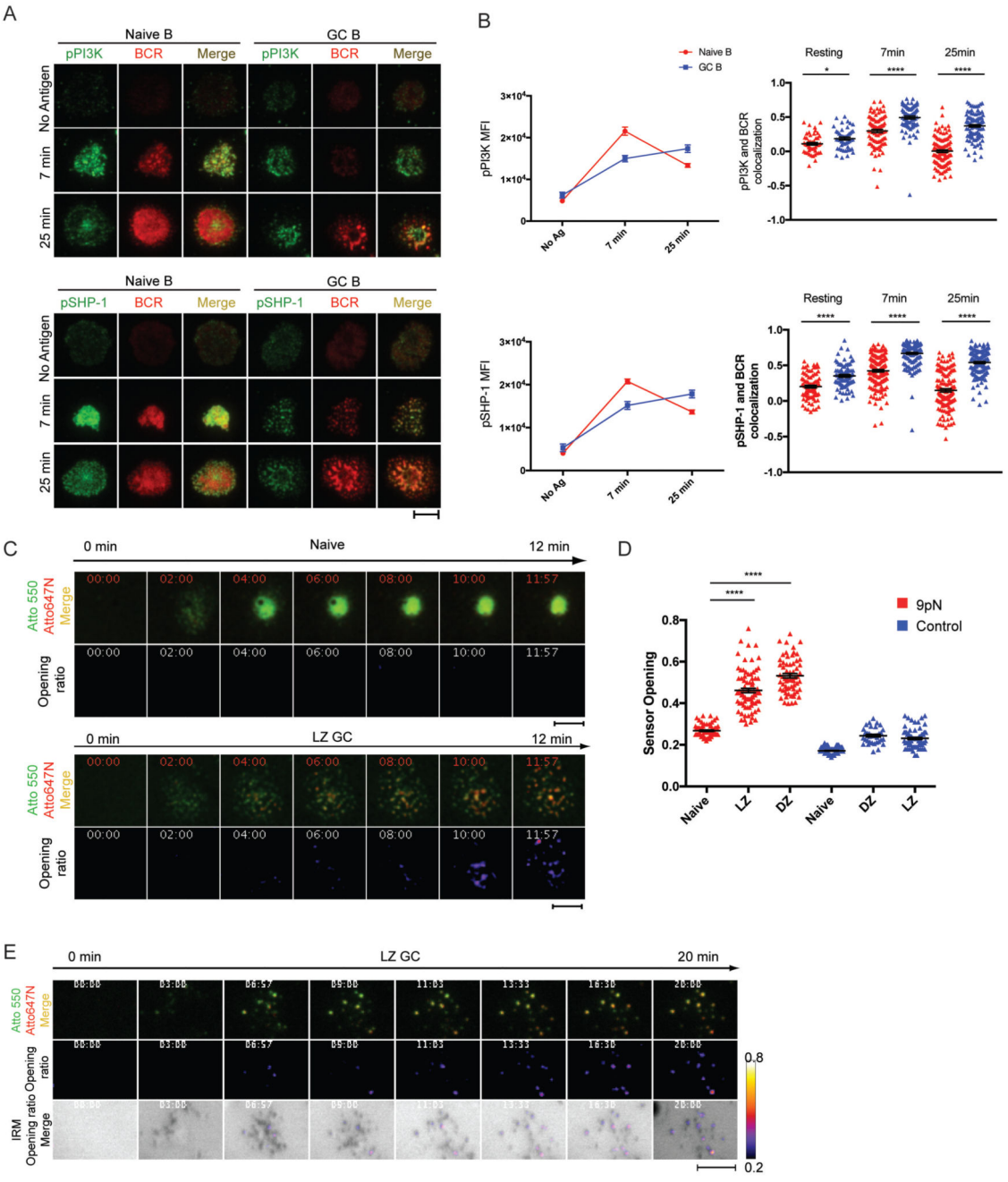

Figure 2.

Human GC B Cells Signal in Response to and Exert Pulling Forces on Membrane Bound Antigens through Pod-like Structures. **(A)** Immune synapses of naïve B cells and GC B cells imaged by TIRFM on PLB containing $F(ab')_2$ anti-λ/κ. **(B)** MFI of pPI3K and pSHP-1 and colocalization of BCR with pPI3K or pSHP-1 in the contact area of naïve and GC B cells placed on antigen-containing PLBs for 7 or 25 min. **(C)** (Top panels) Atto 647N FI (red) and Atto 550 (green) merged images. (Bottom panels) Sensor opening ratio (the ratio of Atto 647N FI to Atto 550 FI). **(D)** Quantification of sensor opening control sensors. **(E)**

Colocalization of sensor opening locations and contact sites to the membrane with time imaged by TIRFM and IRM. Scale bars are 5μm. *ns*>0.05, *$P \leq 0.05$, **$P \leq 0.01$, ***$P \leq 0.001$, and ****$P \leq 0.0001$ (unpaired *t*-test). Data are representative of two experiments. (B and D: mean and s.e.m.)

Europe PMC Funders Author Manuscripts

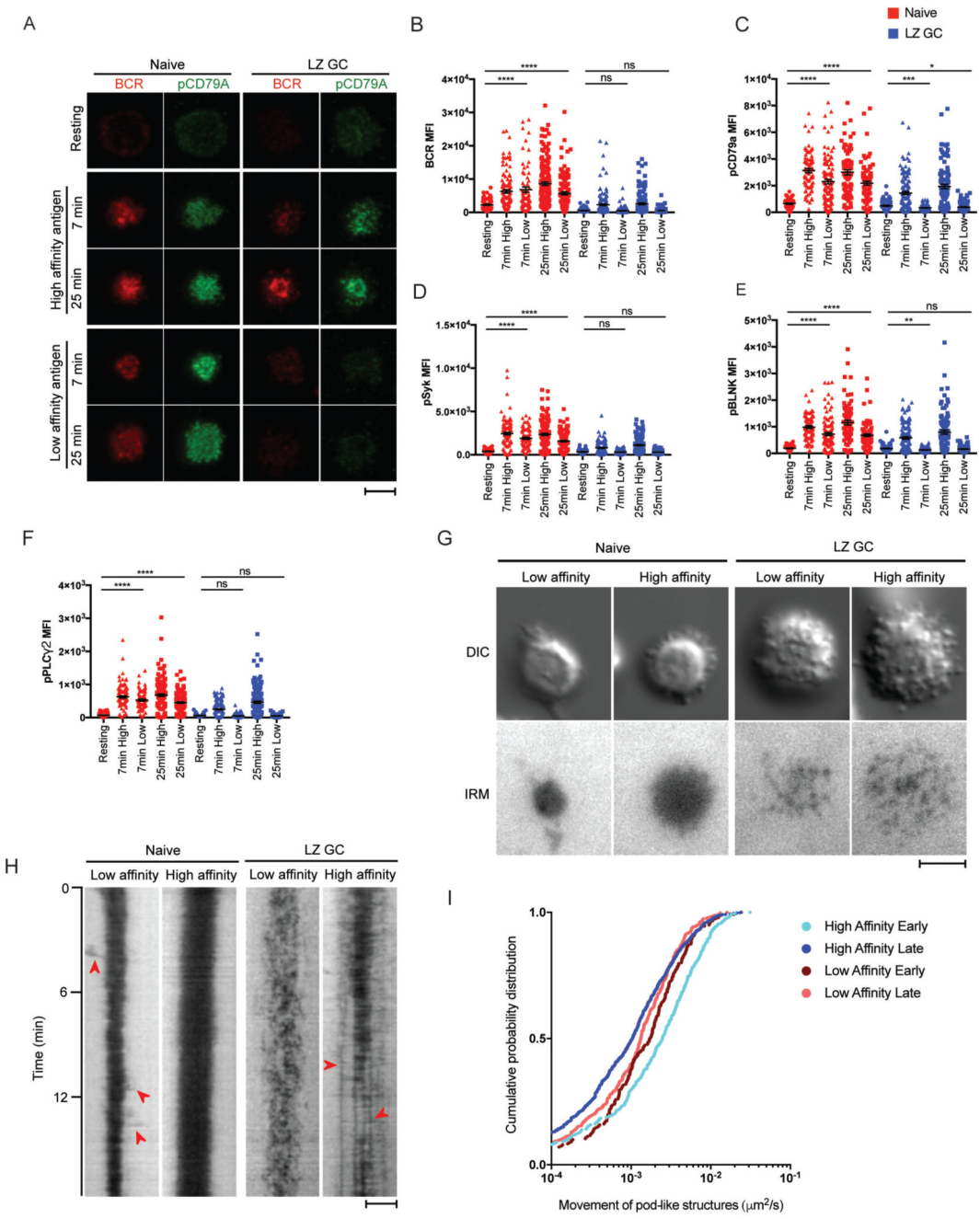

Figure 3.

Human GC B Cells Have a High-Affinity Threshold for Antigen. Naïve and LZ GC B cells were placed on PLB that did not contain antigen (resting) or placed on PLB that contained either high-affinity or low-affinity anti-κ mAbs. **(A)** TIRFM images were obtained of cells stained for the BCR and pCD79A. **(B-C)** Quantification of the BCR (**B**) and pCD79A (**C**) in the contact area of the B cells with the PLB in TIRFM images. **(D-F)** Quantification of TIRF images of cells stained with pSyk (**D**), pBLNK (**E**) and pPLCγ2 (**F**) in the contact area with the PLB of naïve and LZ GC B cells activated by high and low-affinity antigen for 7 or 25

min. **(G)** DIC and IRM images of naïve and LZ GC B cells imaged by TIRFM on PLB containing either high-affinity or low-affinity anti-κ mAbs. The still images were taken between 3 to 12 min of the supplementary movie 6. **(H)** Kymographs of IRM images of naïve and LZ GC B cell immune synapse on low- or high-affinity antigen-containing PLB. Red arrow heads on low-affinity naïve B cell are extended membrane ruffles and on high-affinity LZ GC B cell are pod-like structures established stable contacts to antigen-containing PLB. **(I)** Quantitative analysis of pod-like structure movement in DIC images (number of tracks: n= 347 for high affinity early, n=887 for high affinity late, n=241 for low affinity early, and n=432 for low affinity late). Scale bars are 5μm. *ns*>0.05, ***P*≤0.05, ****P*≤0.01, *****P*≤0.001, and ******P*≤0.0001 (unpaired *t*-test). Data are representative of two experiments. (B-F: mean and s.e.m.)

Europe PMC Funders Author Manuscripts

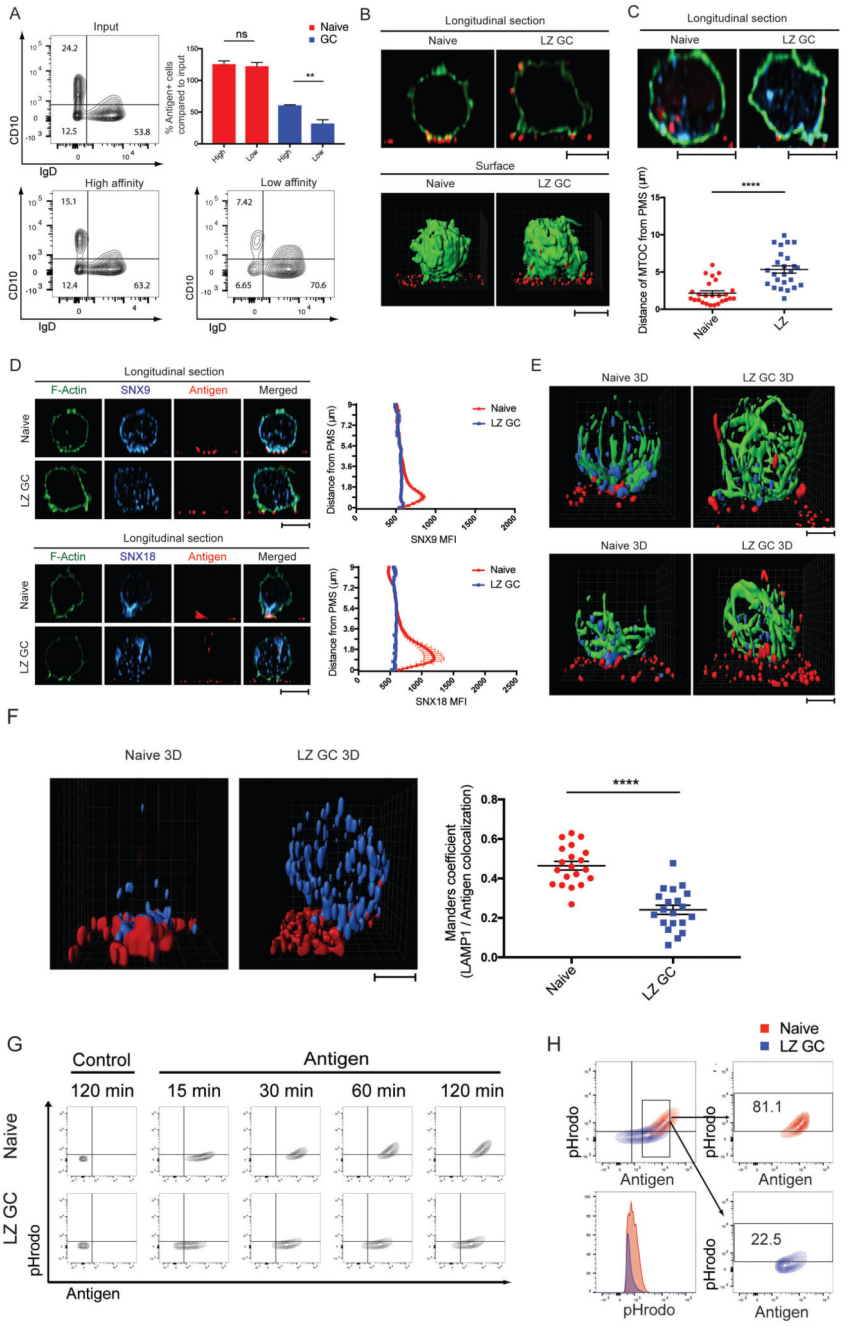

Figure 4.

Extraction and Trafficking of Membrane Associated Antigen Distinguishes GC B cells. **(A)** Antigen extraction by naïve and GC B cells placed for 2 h on PMS that contained either high-affinity or low-affinity anti-κ mAbs. Antigen-positive B cell populations were quantified by flow cytometry. **(B)** Transport of extracted antigens in naïve and LZ GC B cells placed on antigen-containing PMS. F-actin (green) and antigen (red). **(C)** Distance of MTOC in naïve and LZ GC B cells to antigen-containing PMS. F-actin (green), gamma-tubulin (cyan), antigen (red). **(D)** Localization and quantification of SNX9 or SNX18 in

naïve and LZ GC B cells 45 min after activation on antigen-containing PMS imaged by confocal microscopy. F-actin (green), SNX9 and SNX18 (cyan), and antigen (red). MFI of SNX9 and SNX18 per each z-stack from the cell bottom to the top (n=25 per group). **(E)** Localization of SNX9 or SNX18 with MTOC in naïve and LZ GC B cells 45 min after activation on antigen-containing PMS. Alpha-tubulin (green), SNX9 and SNX18 (cyan), and antigen (red). **(F)** Localization pattern of LAMP-1 in naïve and LZ GC B cells (left) 30 min after activation on antigen-containing PMS. 3D colocalization of antigen with LAMP-1 in naïve and LZ GC B cells (right). LAMP-1 (cyan) and antigen (red). **(G)** Trafficking of extracted antigens to acidic intracellular compartments in naïve and LZ GC B cells with time on antigen-containing PMS. **(H)** Percentage of antigen-positive and pHrodo intensities (bottom left) of naïve B cells and LZ GC B cells which are similar in their antigen acquisition. *ns*>0.05, ***P*≤0.05, ****P*≤0.01, *****P*≤0.001, and ******P*≤0.0001 (unpaired *t*-test). Data are representative of two (B-F) or three experiments (A, G, and H). (A, C, D and F: mean and s.e.m.)

Europe PMC Funders Author Manuscripts

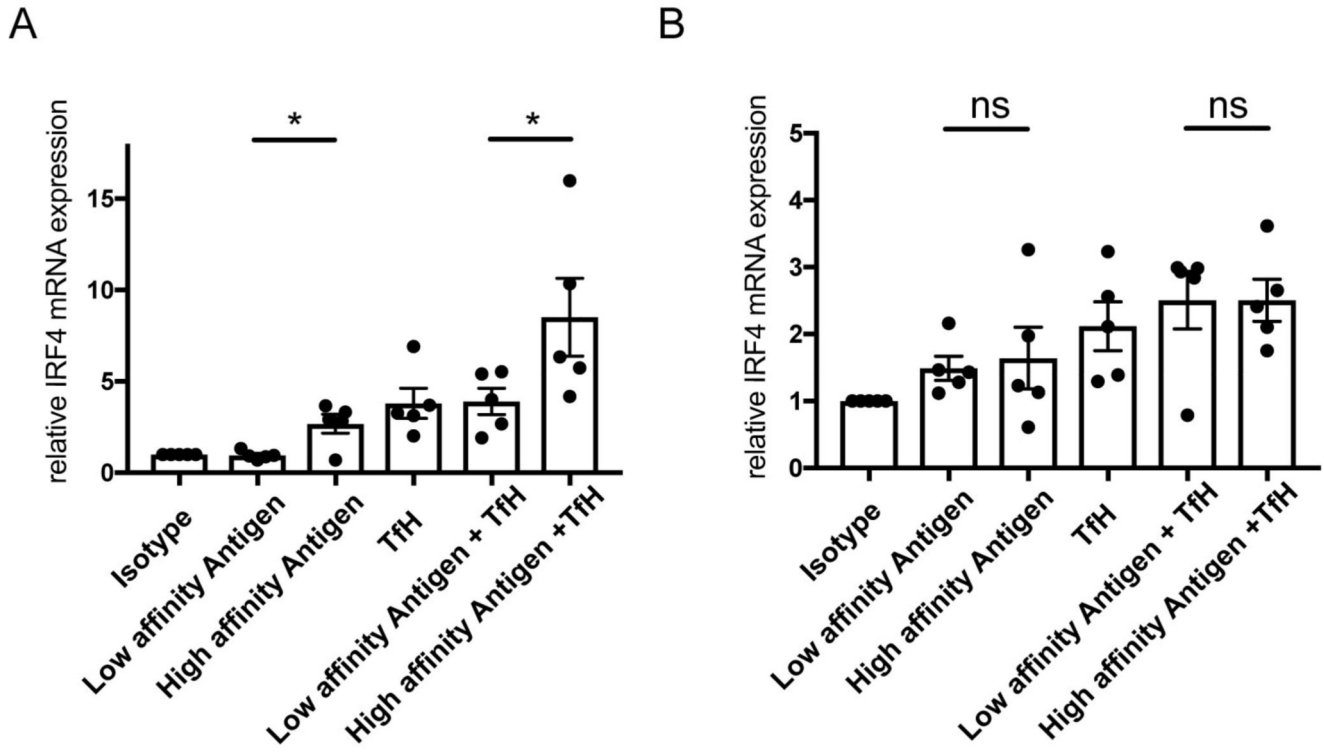

Figure 5.

Human GC B Cells Express IRF-4 in Response to High-Affinity Antigen in Combination with Tfh Cell Help. **(A-B)** Relative mRNA expression level of IRF-4 in LZ GC B (**A**) and naive (**B**) cells after activation with antigens on PLB and/or Tfh like stimuli composed of anti-CD40 mAb, IL-21, and IL-4. *ns*>0.05, ***P*≤0.05, ****P*≤0.01, *****P*≤0.001, and ******P*≤0.0001 (paired *t*-test). (A-B: mean and s.e.m.)

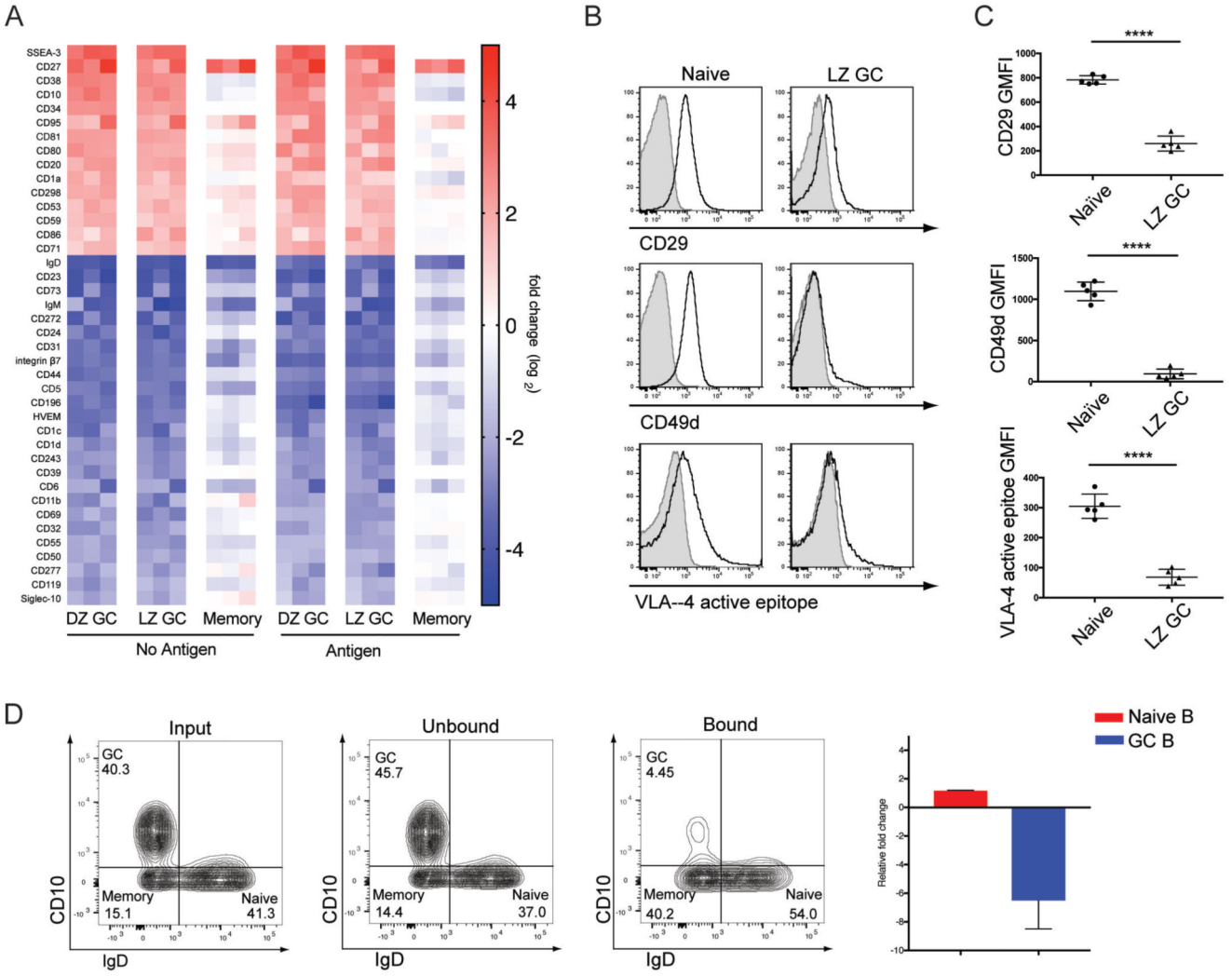

Figure 6.

The Differential Expression of Key Surface Markers may Further Contribute to Affinity Discrimination by Human GC B Cells. **(A)** Heat map: comparisons of differential surface molecule expression **(B-C)** Surface levels of CD29, CD49d, and VLA-4 active epitope in naïve and LZ GC B cells. **(D)** Binding ability of naïve and LZ GC B cells to VCAM-1 coated beads. *ns*>0.05, ***P≤0.05, **P≤0.01, ***P≤0.001, and ****P≤0.0001 (unpaired** *t*-test). Data are from one of five individuals (B) or data are from representative of three experiments (D) (C-D: mean and s.e.m.)

Europe PMC Funders Author Manuscripts